The stochastic enrichment of Population II stars

Louise Welsh,[1][*] Ryan Cooke[1] and Michele Fumagalli[2,1,3]

[1]*Centre for Extragalactic Astronomy, Durham University, South Road, Durham DH1 3LE, UK*
[2]*Dipartimento di Fisica G. Occhialini, Università degli Studi di Milano Bicocca, Piazza della Scienza 3, 20126 Milano, Italy*
[3]*Institute for Computational Cosmology, Durham University, South Road, Durham DH1 3LE, UK*

ABSTRACT

We investigate the intrinsic scatter in the chemical abundances of a sample of metal-poor ([Fe/H] < -2.5) Milky Way halo stars. We draw our sample from four historic surveys and focus our attention on the stellar Mg, Ca, Ni, and Fe abundances. Using these elements, we investigate the chemical enrichment of these metal-poor stars using a model of stochastic chemical enrichment. Assuming that these stars have been enriched by the first generation of massive metal-free stars, we consider the mass distribution of the enriching population alongside the stellar mixing and explosion energy of their supernovae. For our choice of stellar yields, our model suggests that the most metal-poor stars were enriched, on average, by $\hat{N}_{\star} = 5^{+13}_{-3}$ (1σ) Population III stars. This is comparable to the number of enriching stars inferred for the most metal-poor DLAs. Our analysis therefore suggests that some of the lowest mass structures at $z \sim 3$ contain the chemical products from < 13 (2σ) Population III enriched minihaloes. The inferred IMF is consistent with that of a Salpeter distribution and there is a preference towards ejecta from minimally mixed hypernovae. However, the estimated enrichment model is sensitive to small changes in the stellar sample. An offset of ~ 0.1 dex in the [Mg/Ca] abundance is shown to be sensitive to the inferred number of enriching stars. We suggest that this method has the potential to constrain the multiplicity of the first generation of stars, but this will require: (1) a stellar sample whose systematic errors are well understood; and, (2) documented uncertainties associated with nucleosynthetic yields.

Key words: stars: Population III – stars: Population II – stars: abundances – Galaxy: halo – Galaxy: abundances

1 INTRODUCTION

Before the cosmic dawn, essentially all baryons were comprised of hydrogen and helium. The stellar population born from the collapse of this primordial gas transformed their environment irrevocably through the fusion of the first metals (i.e. elements heavier than lithium). As one of the first sources of radiation, these Population III (Pop III) stars were early contributors to the reionisation of the Universe, and, the feedback from these stars influenced the size of the first galaxies (Barkana & Loeb 2001; Bromm & Yoshida 2011). This stellar population is also encoded with vital information such as the size and number abundance of the first star-forming structures in the Universe (i.e. the early dark matter minihaloes) (Abel et al. 2002; Bromm et al. 2002, 2003; Greif et al. 2011; Naoz et al. 2012). Studying this stellar population can therefore shed light on parts of the Universe's history that are currently shrouded in mystery.

In principle, these Population III stars are straight-forward to identify. They are the only stellar population whose atmospheres are expected to be entirely metal-free (at least initially). However,

the search for these stars has spanned almost 4 decades and, as of yet, none have been found (Bond 1980; Beers et al. 1985, 1992; Keller et al. 2007; Christlieb et al. 2008; Aoki et al. 2013; Caffau et al. 2013; Li et al. 2015; Aguado et al. 2016; Howes et al. 2016; Starkenburg et al. 2017; Da Costa et al. 2019). While the first stars have eluded detection, these ongoing surveys have found an ever increasing number of stars that are increasingly deficient in iron. The surviving extremely metal-poor (EMP) stars, whose iron abundances are less than 1/1000 the solar value (i.e. [Fe/H] < -3), are referred to as stellar relics[1]. Their surface abundances are thought to be a window to the chemical composition of the gas from which they formed. Studying the chemistry of these stars may therefore reveal the properties of the stellar population that preceded them. This approach, termed 'stellar archaeology', has become one of the leading observational probes of Population III properties in recent years (Frebel 2010).

---

[1] Here, and throughout this paper, [X/Y] denotes the logarithmic number abundance ratio of elements X and Y relative to their solar values $X_{\odot}$ and $Y_{\odot}$, i.e. [X/Y] = $\log_{10}(N_X/N_Y) - \log_{10}(N_X/N_Y)_{\odot}$.
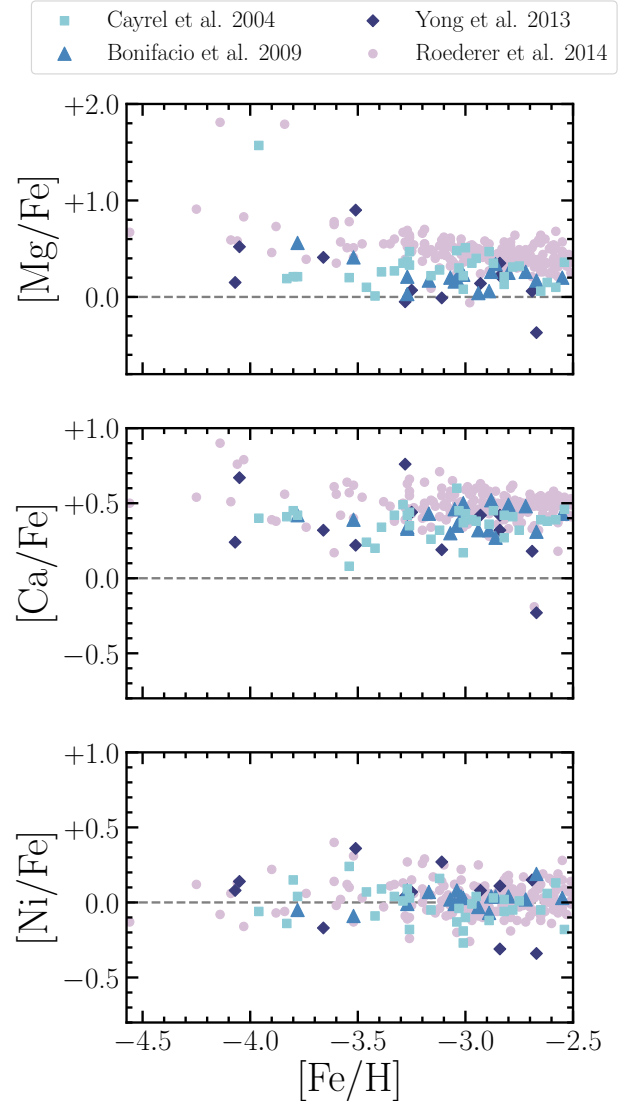
A key property, yet to be uncovered, is the underlying mass distribution of Population III stars. Current simulations suggest that, as these stars formed in the absence of metals, their typical mass range spanned $\sim 10-100\,M_\odot$ (Clark et al. 2008; Stacy et al. 2010; Clark et al. 2011; Greif et al. 2012; Stacy et al. 2016). The Population III initial mass function (IMF) is therefore thought to be distinct from that of later stellar populations. The majority of stars in this expected mass range enrich their environment through core-collapse supernovae (CCSNe). Searches for a Population III signature therefore rely on simulations of stellar evolution, like those of Woosley & Weaver (1995); Umeda & Nomoto (2002, 2003); Chieffi & Limongi (2004); Umeda & Nomoto (2005); Tominaga et al. (2007); Heger & Woosley (2010); Limongi & Chieffi (2012), to compare the chemical abundances expected from Population III CCSNe to those observed in the atmospheres of surviving Population II stars.

Carbon-enhanced ([C/Fe] > +0.7) EMP stars that show 'normal' relative abundances of neutron-capture elements (i.e. CEMP-no stars) are considered to be the most likely descendants of the first stars (Beers & Christlieb 2005; Frebel & Norris 2015). It has been suggested that the CEMP-no stars in the metallicity regime $-5 <$ [Fe/H] < -4 are the most promising probes of Population III properties (Placco et al. 2016). However, only 11 stars are currently known to meet this criteria[2]. It is also unclear what fraction of Population II stars are likely to present as CEMP-no stars in the local Universe (Ji et al. 2015; Hartwig & Yoshida 2019). Thus, searches for a Population III chemical signature generally include EMP stars alongside CEMP-no stars.

Cosmological hydrodynamic simulations have suggested that Population III stars likely formed either individually or in small multiples (Greif et al. 2010; Stacy et al. 2010; Susa et al. 2014). However, traditional comparisons between the observed stellar abundances and the simulated yields have been restricted to two scenarios, either: (1) one progenitor is responsible for the enrichment of a surviving star (e.g. Frebel et al. 2015; Nordlander et al. 2019; Ezzeddine et al. 2019); or (2) the observed abundances can be modelled by the IMF weighted yields from these simulations (e.g. Heger & Woosley 2010; Yong et al. 2013; Ishigaki et al. 2018). Though, the use of semi-analytic models has enabled the consideration of multiple enriching progenitors (Karlsson 2005; Karlsson & Gustafsson 2005; Hartwig et al. 2018a).

In this paper, we use a novel approach to analyse the chemistry of the most metal-poor stars, and use this tool to infer the number of massive Population III stars that have enriched the surviving metal-poor stellar relics. Previously, we have applied this tool to investigate the enrichment of the *most* metal-poor damped Lyman-α systems (DLAs) (Welsh et al. 2019, 2020). We now extend this work to investigate the stochastic enrichment of a sample of metal-poor Milky Way halo stars using their measured [Mg/Ca] and [Ni/Fe] abundances. While not the subject of this work, we note that the potential for inhomogeneous metal-mixing at the sites of Population II star formation is an additional complication that is an interesting avenue for further investigations (Salvadori et al. 2010; Sarmento et al. 2017; Hartwig et al. 2018b; Tarumi et al. 2020).

Our paper is organised as follows. Section 2 describes the observational sample used in this paper. Section 3 motivates the use of a stochastic enrichment model. In Section 4 we outline this model

---

[2] As documented by the Stellar Abundances for Galactic Archaeology (SAGA) database — an invaluable tool for exploring and compiling stellar samples from existing surveys of metal-poor stars (Suda et al. 2008, 2011; Yamada et al. 2013; Suda et al. 2017).

Figure 1. From top to bottom, the successive panels show the measured [Mg/Fe], [Ca/Fe], and [Ni/Fe] abundances of our stellar sample as a function of their [Fe/H] abundances. The colour and shape of the marker indicate the source of the data (defined in the legend and used throughout this paper). The horizontal dashed line indicates the solar value. Note the different y-axis scale used in the top panel.

and apply it to the observational data. The results are discussed in Section 5 before drawing overall conclusions in Section 6.

2 DATA

The stellar abundances considered in this work are a compilation of four sources. Specifically, that of: Cayrel et al. (2004; hereafter C04), Bonifacio et al. (2009; hereafter B09), Yong et al. (2013; hereafter Y13), and, Roederer et al. (2014; hereafter R14). C04 and B09 are part of the *First Stars* series. Note that we only consider the programme stars reported by Y13 (and not the literature stars used in their analysis). A summary of these data can be found in Table 1 where programme size indicates the number of stars reported in the

Table 1. Summary of surveys that we consider in this work.

survey	programme size	sample size	N_{giants}	σ_{Mg}	σ_{Ca}	σ_{Ni}
C04	35	32	32	0.12	0.11	0.06
B09	19	18	0	0.06	0.11	0.07
Y13	38	12	5	0.11	0.12	0.15
R14	313	188	92	0.19	0.20	0.22

Table 2. Solar abundances adopted in this analysis and those used in sample sources.

Element	This Work	C04	B09	Y13 / R14
Mg	7.56	7.58	7.58	7.60
Ca	6.29	6.36	6.36	6.34
Fe	7.47	7.50	7.51	7.50
Ni	6.21	6.25	6.25	6.22

original works, sample size indicates the number of objects used in our analysis, and σ_X indicates the median error associated with the reported [X/Fe] values. Across all samples there are 11 metals in common[3]. In our paper, we restrict our analysis to the Mg, Ca, Fe, and Ni abundances of these samples. The choice of elements is primarily driven by the perceived confidence in both the observed abundances and the simulated yields. Furthermore, the abundances of these elements are commonly reported in stellar samples, and are sensitive to the properties (e.g. mass) of the stars that synthesised these elements.

The abundances adopted in our work have been computed under the assumption of local thermodynamic equilibrium (LTE) using 1D model atmospheres. These models do not capture possible spatial inhomogeneities. Mg, Ca, and Ni abundances are often determined from the spectral features of neutral species; these lines are generally thought to be more susceptible to non-LTE processes than those of ionised species (Asplund 2005). We do not apply non-LTE corrections to these data, but the impact of this decision is discussed in Section 5.1. Similarly, Fe I lines are known to be affected by ove-rionisation (Thévenin & Idiart 1999). This can in-turn impact the estimated surface gravity of the star. These departures from LTE are often accounted for through comparisons of the Fe I and Fe II abundances. We note that this correction may be imperfect as Fe II lines may also form in regions that depart from LTE.

We apply a metallicity cut at [Fe/H] < −2.5. This ensures our sample of metal-poor halo stars is of comparable metallicity to the sample of DLAs analysed by Welsh et al. (2019). This criteria is more lax than the limit commonly imposed when investigating Population II chemical enrichment; these studies often reserve their analysis for EMP stars with [Fe/H] < −3. These stars are considerably less numerous and are often analysed individually; including these stars, from additional sources, would risk biasing our sample towards the *most* chemically peculiar stars currently known. As summarised in Table 1, we consider 32 stars from C04, 18 stars from B09, 12 stars from Y13, and 191 stars from R14. This sample contains stars in various stages of their evolution. We make no initial distinction between the abundances of giants and non-giants. Figure 1 shows the abundances of these survey stars as a function of their [Fe/H] abundance. Note that to be included in our sample, a star must be sufficiently metal poor ([Fe/H] < −2.5) and have bounded [Mg/Fe], [Ca/Fe], and [Ni/Fe] abundances (i.e. we ignore stars with upper abundance limits). The solar values adopted in this paper are taken from Asplund et al. (2009) and are shown in Table 2 alongside those adopted by the original sources. Note that all of the measured abundances and chemical yields that are used in this work have been registered onto the same solar abundance scale (see second column of Table 2).

To investigate the properties of Population III stars using the chemical abundances of Population II stars, we require a ho-

mogeneous stellar sample whose photospheric abundances are not dominated by systematic effects. As highlighted in Figure 1, the R14 data is known to show an elevated [Mg/Fe] abundance relative to the other samples. The origin of this offset, as found by R14, is due to the way that the effective temperature T_{eff} is determined. C04, B09, and Y13 each utilise a combination of photometric and spectroscopic information to determine T_{eff}. R14 exclusively consider spectroscopic data in their determination of T_{eff}. We find that this offset between the R14 data and the other samples can be minimised when considering the abundance ratios of elements close to one another in atomic number — in this case [Mg/Ca] and [Ni/Fe]. The generalised histograms of these abundance ratios for each sample is show in Figure 2. When comparing the abundances of these stars to the yields of Population III SNe, we therefore draw parallels between the observed and simulated [Mg/Ca] and [Ni/Fe] abundances. This allows us to consider the stars from all four surveys simultaneously and take advantage of the large dataset afforded by R14. We note that there are a number of stars that appear in multiple surveys. For these objects, we adopt the abundances derived from data with the superior spectral resolution. The numbers quoted in Table 1 represent the data after the removal of duplicates; there are therefore 250 unique stars in this sample.

3 INTRINSIC SCATTER

Before we model the chemical enrichment of these data in detail, we first motivate the importance of employing a stochastic chemical enrichment model given the present sample of stars. Treating each stellar survey independently, we have investigated if the reported abundances show significant *intrinsic* scatter that cannot be explained by the observational errors. To quantify this additional scatter, we model each abundance ratio as a Gaussian centred about [X/Fe]$_{cent}$ whose error is given by the expression:

$$\sigma_{tot}^2 = \sigma_{obs}^2 + \sigma_{int}^2 . \tag{1}$$

Thus, the dispersion of the data is given by the observed error σ_{obs} and an additional intrinsic component σ_{int} added in quadrature. We therefore consider two model parameters ([X/Fe]$_{cent}$ and σ_{int}) that we determine independently for each abundance ratio and each sample.

When looking at the [Mg/Fe], [Ca/Fe], and [Ni/Fe] abundances of the individual surveys, we have consistently found a non-zero intrinsic scatter associated with the [Mg/Fe] abundances of all the stellar samples. This intrinsic scatter is estimated using a Markov Chain Monte Carlo (MCMC) procedure that simultaneously estimates the central values [Mg/Fe]$_{cent}$, [Ca/Fe]$_{cent}$, and [Ni/Fe]$_{cent}$ of a sample, alongside their associated additional error components $\sigma_{int,Mg}$, $\sigma_{int,Ca}$, and $\sigma_{int,Ni}$. For details of this calculation and an example of the converged analysis of the C04 data, see Appendix A. Figure 3 shows the resulting posterior distributions of this analysis for all stellar samples used in this work. The bottom left panel of

---
[3] These elements include: C, Mg, Si, Ca, Sc, Ti, Cr, Mn, Fe, Co, and Ni.
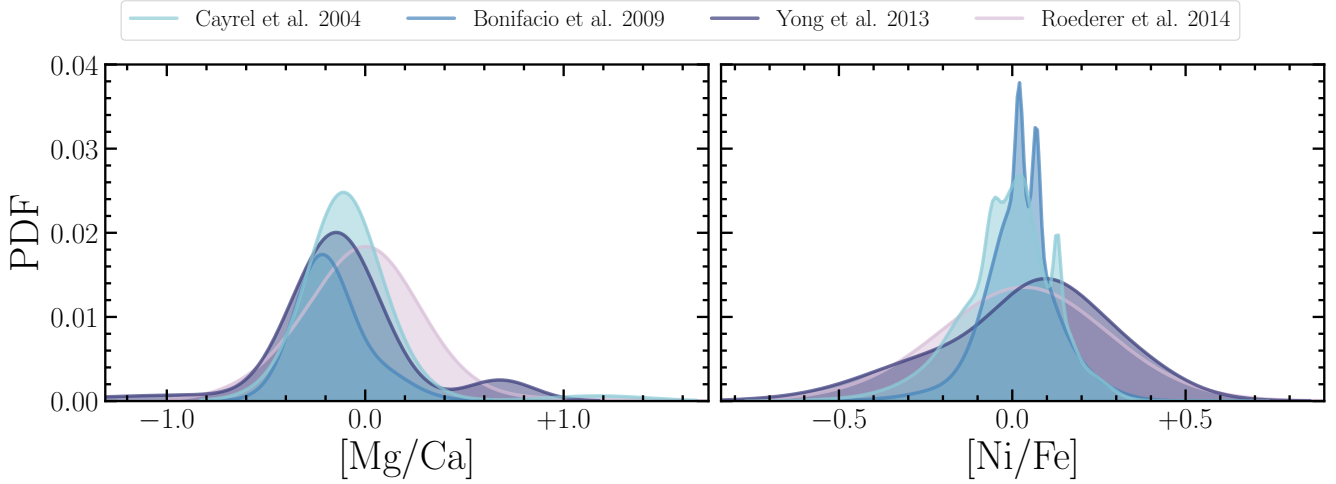
Figure 2. Generalised histograms showing the [Mg/Ca] (left) and [Ni/Fe] (right) abundance distributions of the individual samples. The colour indicates of the source of the data. The chemical abundance of each object has been treated as a Gaussian with a standard deviation given by the observational error. Considering the abundance ratios of elements close to one another in atomic number minimises the differences seen between the samples.
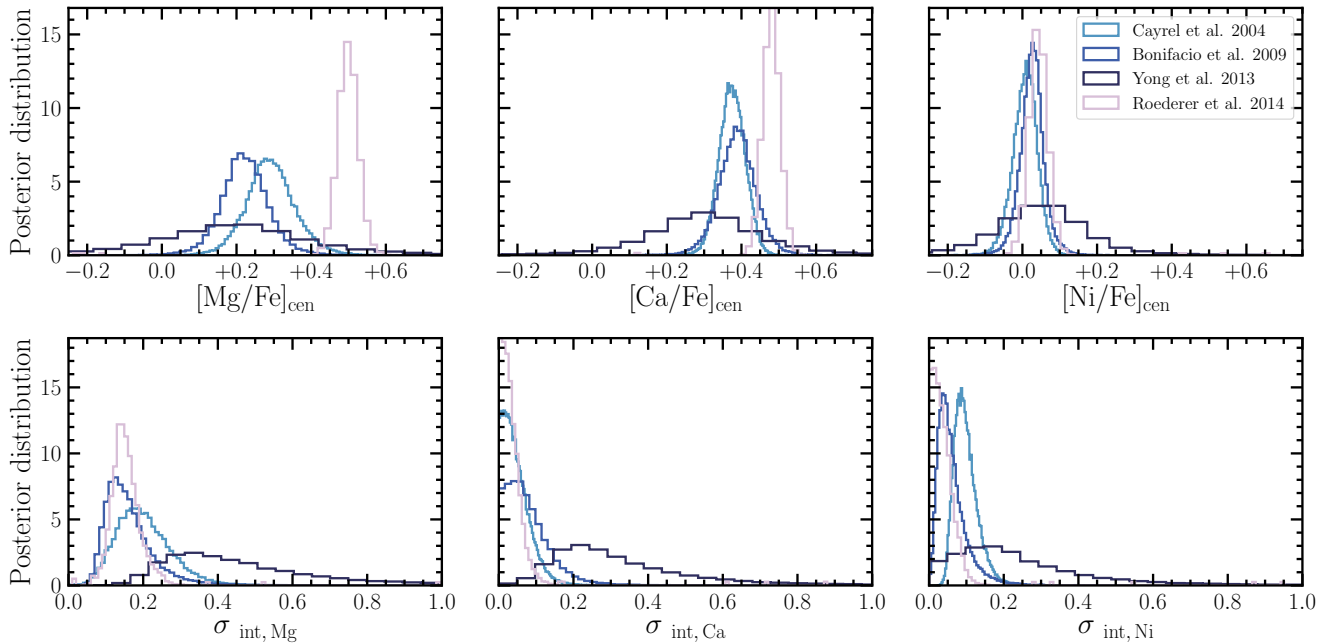
Figure 3. The top row shows the posterior distributions of the central [Mg/Fe] (left), [Ca/Fe] (centre), and [Ni/Fe] (right) abundance ratios estimated for each survey independently. The bottom row shows the posterior distributions of the intrinsic scatter associated with these central values. The colour of the histogram indicates the source of the data (as indicated in the legend).

this figure shows the posterior distribution of the intrinsic scatter present in the [Mg/Fe] data. This intrinsic scatter implies that either: (1) there is a consistent intrinsic scatter associated with the [Mg/Fe] abundances of the stars in every sample; or (2) the [Mg/Fe] abundance errors are all consistently underestimated by ~ 0.15 dex. In this paper, we consider the first possibility, but note that there may also be some non-physical origin of this scatter. For example, the impact of assuming LTE may affect stars of a given metallicity, temperature, and/or surface gravity more significantly than others.

We have repeated this analysis after removing the peculiar stars with [Mg/Fe]> +1 (see the top panel of Figure 1). This modification affects both the C04 and R14 data. We find that the estimated intrinsic scatter is reduced across both samples; for the R14 sample, the revised intrinsic scatter is consistent with zero, whereas the C04 sample supports a statistically significant deviation (2σ) from zero intrinsic scatter. We have also investigated whether this scatter is dependent on the metallicity of the star. Focusing on the C04 sample, we found that the enhanced [Mg/Fe] abundance of CS 22949 − 037
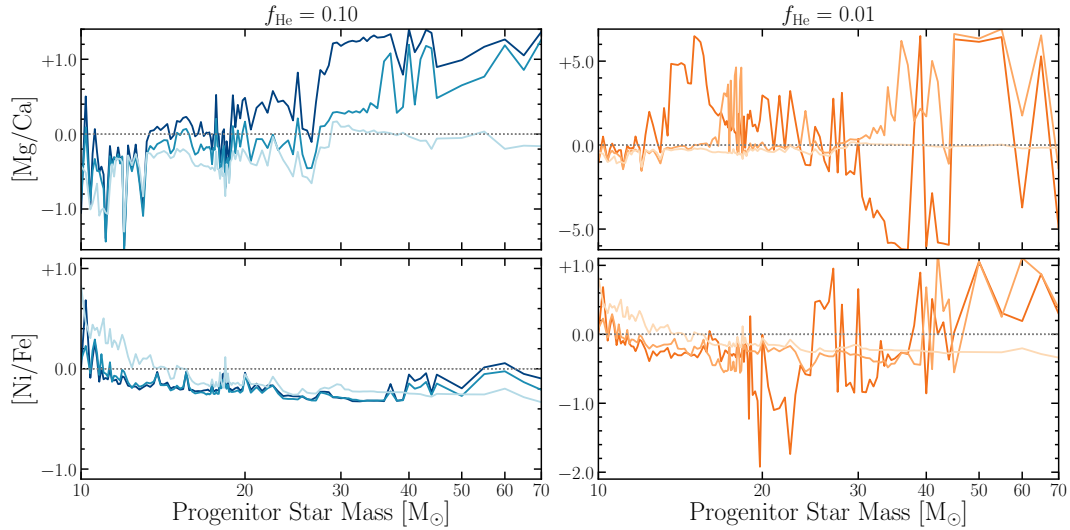
Figure 4. [Mg/Ca] and [Ni/Fe] yields as a function of the progenitor star mass for a range of stellar properties. As indicated by the title, the two left-hand panels show the yields associated with stars that undergo the fiducial amount of mixing between stellar layers (10 per cent of the He core size). The progressively lighter blue lines correspond to progressively more energetic explosions. Specifically, dark to light shades highlight a 0.9, 1.8, and 10 B explosion, respectively. The orange lines in the right-hand panels highlight the variability of the yields when a star experiences minimal mixing between the stellar layers (1 per cent of the He core size). The progressively lighter orange lines correspond to the same change in explosion energy. Finally, the horizontal dotted line indicates the solar abundance of these abundance ratios.

is difficult to replicate alongside the other data. If it is removed from the sample, we find no strong dependence with metallicity. The result is mirrored when considering the R14 data. The B09 and Y13 samples are deemed too small to reliably capture any relationship between the intrinsic scatter and the metallicity of a star.

We emphasise that, irrespective of trends with metallicity, the intrinsic scatter in [Mg/Fe] is non-negligible for each sample when treated independently. The scatter in this data may highlight the inhomogeneous nature of the environments within which these stars formed. To understand the chemical abundances of these objects it is therefore necessary to consider a stochastic chemical enrichment model.

4 STOCHASTIC ENRICHMENT

Using a model of stochastic chemical enrichment in combination with the yields from simulations of stellar evolution, we can test if the observed chemical abundances of Population II stars are consistent with enrichment by Population III SNe. This model assumes that the number of Population III stars responsible for enriching a given environment is given by the integral:

$$N_\star = \int_{M_{\min}}^{M_{\max}} k M^{-\alpha} dM \qquad (2)$$

where M is the mass of the Population III star, α controls the slope of the power-law, and k is a multiplicative constant dependent on the number of stars forming within the mass range bounded by $M_{\min}$ and $M_{\max}$. In addition to the mass distribution of the enriching stars, we consider the typical explosion energy of the Population III SNe as well as the degree of mixing between the stellar layers. To determine the abundances expected from a given model, we rely on simulations of stellar evolution. Our fiducial choice of nucleosynthetic yields, described below, are those of Heger & Woosley (2010; hereafter HW10).

The HW10 simulations calculate the yields of massive Population III stars that end their lives as Type II SNe. This simulation suite reports a grid of chemical yields as a function of: (1) the progenitor star mass; (2) the mixing between the stellar layers during the explosion, and; (3) the kinetic energy of the SNe ejecta at infinity. These yields have been calculated using non-rotating, 1D models under the assumption of spherical symmetry. They do not account for mass loss or magnetic fields. The Rayleigh-Taylor instabilities that aide mixing between the stellar layers cannot be captured by 1D models. In these simulations mixing is achieved by moving a boxcar of width ΔM through the star, typically four times. ΔM is described as a fraction of the He core size f_{He}. The boxcar width that reproduces the hard X-ray and optical lightcurves of SN 1987A is 10 per cent of the He core size ($f_{\mathrm{He}} = 0.100$). The eventual collapse of the progenitor, and the subsequent SN explosion, is simulated by depositing momentum at the base of the oxygen burning shell. The strength of this explosion is parameterized by the kinetic energy of the ejecta at infinity. The typical explosion energy of a SN is $E_{\exp} = 1$ B (where 1 B = 10^{51} ergs). The HW10 yields have been calculated for 16,800 combinations of these three parameters (progenitor mass, stellar mixing, and explosion energy).

Figure 4 shows the yields of [Mg/Ca] and [Ni/Fe] as a function of progenitor star mass for a range of explosion energies. The left and right set of panels show the simulated yields for two mixing prescriptions. Those on the left adopt the value recommended by HW10 (10 per cent of the He core size). Those on the right indicate the yields of SNe that undergo minimal mixing between stellar layers (1 per cent of the He core size). From this figure it is clear that the yields of both [Mg/Ca] and [Ni/Fe] are highly variable for low values of the SNe explosion energy and/or the mixing width. There is a more consistent relationship with progenitor mass when $f_{\mathrm{He}} = 0.1$. In this case, there is a general trend of increasing [Mg/Ca] with increasing progenitor mass, while [Ni/Fe] shows no strong evolution across the considered mass range.
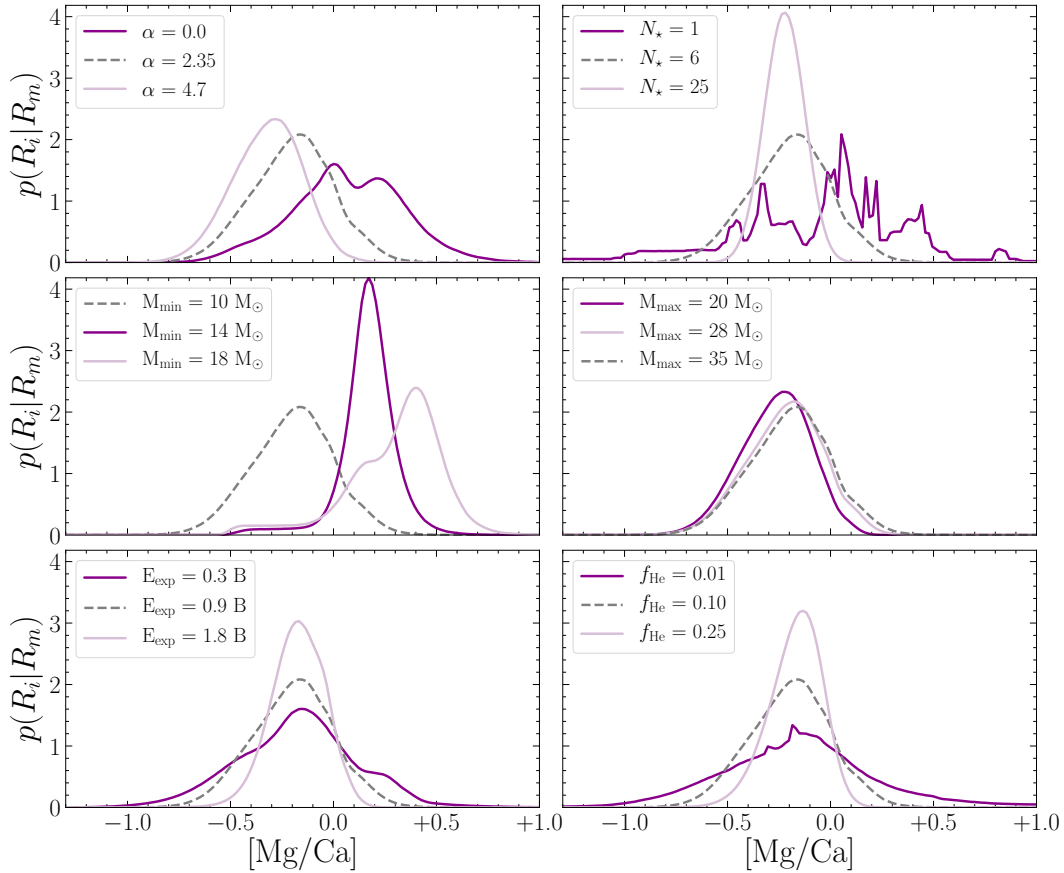
Figure 5. Probability distribution of the intrinsic [Mg/Ca] ratio that would be expected for a range of underlying enrichment models. From top left to bottom right, the successive panels correspond to changing the slope, number of enriching stars, minimum mass, maximum mass, explosion energy, and degree of mixing. Unless otherwise stated in the legend, the model parameters of these distributions are $\alpha = 2.35$, $N_\star = 6$, $M_{\mathrm{min}} = 10\,\mathrm{M}_\odot$, $M_{\mathrm{max}} = 35\,\mathrm{M}_\odot$, $E_{\mathrm{exp}} = 0.9$ B, and $f_{\mathrm{He}} = 10$ per cent (displayed as the grey dashed line in all panels as a point of comparison).

4.1 Stochastic sampling

To determine how the simulated Population III yields compare to the observed abundances of stellar relics, it is necessary to consider how these objects may have been chemically enriched. In their respective minihaloes, the first stars are thought to form either individually or in small multiples. Thus, the surviving Population II stars may have been enriched by the chemical products of multiple SNe. The progenitors of these SNe formed obeying an underlying mass distribution. Given the small number of Population III stars forming in each minihalo, this mass distribution would have necessarily been stochastically sampled. The relative abundances of the stellar population enriched by Population III SNe may therefore show an intrinsic spread.

For any given enrichment model, we would like to calculate the probability of observing each star in our sample. The probability of observing a given abundance pattern (e.g. [Mg/Ca] and [Ni/Fe]) is

$$p_n(R_o|R_m) = \int p(R_o|R_i)p(R_i|R_m)\mathrm{d}R_i \ . \tag{3}$$

The first term of this integral describes the probability of *observing* a given abundance pattern (R_o) given the intrinsic abundance ratios of the system, R_i. In other words, this variable describes how close the observed measurement is to the true value. We model each abundance ratio by a Gaussian whose spread is given by the

observational error. The second term of this integral describes the probability of obtaining an intrinsic abundance pattern given the stochastic enrichment model defined by Equation 2.

To determine the expected distribution of relative abundances given an enrichment model (i.e. $p(R_i|R_m)$), we construct a grid of IMF model parameters, and sample each grid point 10^3 times. For each iteration, we use the sampled stellar masses to determine the yields of the associated SNe. It is assumed that the SNe ejecta are well-mixed. The resulting number abundance ratio of [Mg/Ca], for example, is therefore given by the total yield of Mg relative to the total yield of Ca from all of the sampled stars. Using this Monte Carlo sampling technique, we can build an N-dimensional probability density function of the expected yields, where N is the number of abundance ratios under consideration. In this work we consider the [Mg/Ca] and [Ni/Fe] abundance ratios (thus, $N=2$).

In this work, $p(R_i|R_m)$ describes the joint probability of simultaneously producing any given combination of [Mg/Ca] and [Ni/Fe]. Figure 5 illustrates how the different enrichment model parameters influence the expected distribution of [Mg/Ca]. The successive panels correspond to changing the slope, number of enriching stars, minimum mass, maximum mass, explosion energy, and stellar mixing, respectively. The fiducial model parameters used in Figure 5 (grey-dashed curves) are: $\alpha = 2.35$, $N_\star = 6$, $M_{\mathrm{min}} = 10\,\mathrm{M}_\odot$, $M_{\mathrm{max}} = 35\,\mathrm{M}_\odot$, $E_{\mathrm{exp}} = 0.9$ B, and $f_{\mathrm{He}} = 10$ per cent. From this figure it is clear that the expected distributions of intrinsic abun-

dances are sensitive to the average number of Pop III stars that enriched the second generation of stars. Thus, given an appropriate sample of observed stellar abundances, this model can be used to estimate the average number of Population III SNe that have chemically enriched the surviving Population II stars. Under the assumption that each surviving star is enriched by the well-mixed SNe ejecta from one minihalo, this analysis can be used to gauge the multiplicity of the first stars.

4.2 Likelihood analysis

The likelihood of an enrichment model is given by:

$$\mathcal{L} = \prod_n p_n(R_o|R_m)\,, \tag{4}$$

To estimate the enrichment model parameters that provide the best fit to the observed abundances, we utilise the EMCEE software package (Foreman-Mackey et al. 2013) to conduct an MCMC likelihood analysis. In this analysis, we adopt uniform priors across all of the model parameters bounded by:

$$
\begin{aligned}
1 &\leq & N_\star & \leq 100\,, \\
-5 &\leq & \alpha & \leq 5\,, \\
20 &\leq & M_{\max}/M_\odot & \leq 70\,, \\
0.3 &\leq & E_{\exp}/10^{51}\mathrm{erg} & \leq 10\,, \\
0 &\leq & f_{\mathrm{He}} & \leq 0.25\,.
\end{aligned}
$$

These boundary conditions are chosen to cover the physically motivated parameter space, given our assumptions about Population III star formation. The number of massive stars that chemically enrich their environment via CCSNe is expected to be small. The slope of the power-law that dictates Population III star formation is still unknown, we therefore have parameterised the IMF of massive stars ($M > 10\ M_\odot$) as a power-law IMF, which is consistent with the shape found in the local Universe. The slope of this power-law for local star formation is given by $\alpha = 2.35$ (Salpeter 1955; see Bastian et al. 2010 for a review). The minimum mass of the enriching stars is fixed at $M_{\min} = 10\ M_\odot$ as it is assumed that all stars above this mass limit are capable of undergoing core-collapse. The upper bound on the mass of the enriching stars coincides instead with the onset of pulsational pair instability SNe (Woosley 2017). The boundary conditions on both the average SN explosion energy and mixing prescription cover all of the values explored in HW10. These simulations calculated the SNe yields for discrete combinations of M, $E_{\exp}$, and f_{He}; we linearly interpolate over this 3D parameter space for our analysis.

Similar to the approach from Welsh et al. (2019, 2020), we begin our analysis with 400 randomly initialised walkers. These walkers each take 10 000 steps to converge on the stable posterior distributions shown in Figure 6. The grey contours highlight the result of considering all of the stars in our chosen sample. We find that the mass distribution of the enriching Population III stars is broadly consistent with a Salpeter ($\alpha = 2.35$) IMF; however, the bottom-heavy tail of the distribution is poorly constrained. Similarly, the maximum mass of the enriching stars is largely unconstrained, while showing a slight preference towards higher values. This analysis suggests that the enriching progenitors have experienced minimal mixing between stellar layers ($f_{\mathrm{He}} \sim 0.03$). The remaining parameters, $N_\star$ and $E_{\exp}$, show two possible scenarios. If $N_\star < 20$ then the yields of hypernovae ($E_{\exp} \sim 8$ B) are most suitable. Alternatively, if $N_\star > 30$, we find that these Population II stars are best modelled with the yields of weak ($E_{\exp} \sim 0.3$ B) Population III SNe. This

latter scenario is consistent with the result of HW10 (see their figure 12). If we repeat this analysis after removing the R14 data (see the blue contours in Figure 6), these two scenarios persist. However, there is a clear preference towards the low $N_\star$ scenario that, in this case, also coincides with an unconstrained mixing prescription. Removing the R14 data reduces the allowed parameter space of our model, even though the observed distributions of [Mg/Ca] and [Ni/Fe] of each independent survey are broadly consistent (see Figure 2). This highlights that the estimated model parameters are sensitive to small differences in the observationally measured abundances. Before we investigate the potential origins of this difference, we note that repeating our analysis using only the abundances of the 129 giants in our sample (defined as those with log $g < 3$) has a negligible impact on our parameter estimates. Similarly, removing potentially peculiar stars with elevated Mg ([Mg/Fe] > +1) does not change the parameter estimates. This is not surprising, as the majority of the stars in our sample have [Mg/Fe] < +1 (see Figures 1 and 2).

4.3 Maximum likelihood results

To investigate the quality of the estimated enrichment models, we use the posterior distributions of the model parameters to generate the expected stellar abundances of [Mg/Ca] and [Ni/Fe]; we then compare these distributions to the observed abundances of the stellar sample. This exercise indicates that our inferred model parameters, based on the C04, B09, Y13, and R14 samples, does not encompass the full extent of the data. In particular, Figure 7 highlights a bimodal distribution of [Ni/Fe], which is a result of the bimodal distribution of $E_{\exp}$ (and hence $N_\star$) seen in Figure 6. As can be seen in Figure 4, there are a range of models that can capture the [Ni/Fe] range seen in the data ($-0.4 \lesssim$ [Ni/Fe] $\lesssim +0.4$), including minimally mixed weak SNe and high energy SNe with 'normal' mixing. However, these two possible ways to explain the broad [Ni/Fe] distribution are unable to simultaneously reproduce the observed [Mg/Ca] distributions. In particular, our model does not simultaneously favour supersolar [Mg/Ca] and [Ni/Fe] abundances. This highlights the importance of simultaneously modelling the interdependence of the $p(R_i|R_m)$ distributions for all elements being considered in a stochastic enrichment model, as discussed in Section 4.1.

From Figure 8, we can see that the distinction between the model and observed distributions are less pronounced when we repeat our analysis after removing the R14 data. The R14 data comprise most of our sample, and exhibit somewhat elevated [Mg/Ca] values, compared with the rest of the sample (see Figure 1). While this offset is ~ 0.1 dex, it is large enough to affect the parameter constraints of our model. We therefore conclude that our stochastic chemical enrichment model is able to reproduce the observations if we exclude the R14 data. As discussed in Section 2, the somewhat elevated Mg abundances reported by R14 are due to their adopted approach for estimating the effective temperature. Going forward, it is clear that the relative element abundance measurements need to be reported with an accuracy of better than ~ 0.05 dex.

Given that our model is able to reproduce the observations when we exclude the R14 data (see Figure 8), we favour the maximum likelihood results of our model parameters based on the C04, B09, and Y13 combined sample. We find that the average number of massive Population III stars that best describe the observed [Mg/Ca] and [Ni/Fe] abundances of these Population II stars is $\hat{N}_\star = 5^{+13}_{-3}$ where the quoted errors, here and subsequently, are the 68 per cent confidence region associated with the maximum likelihood value. These stars form obeying a power-law IMF with a slope $\hat{\alpha} = 2.9^{+0.9}_{-0.6}$.
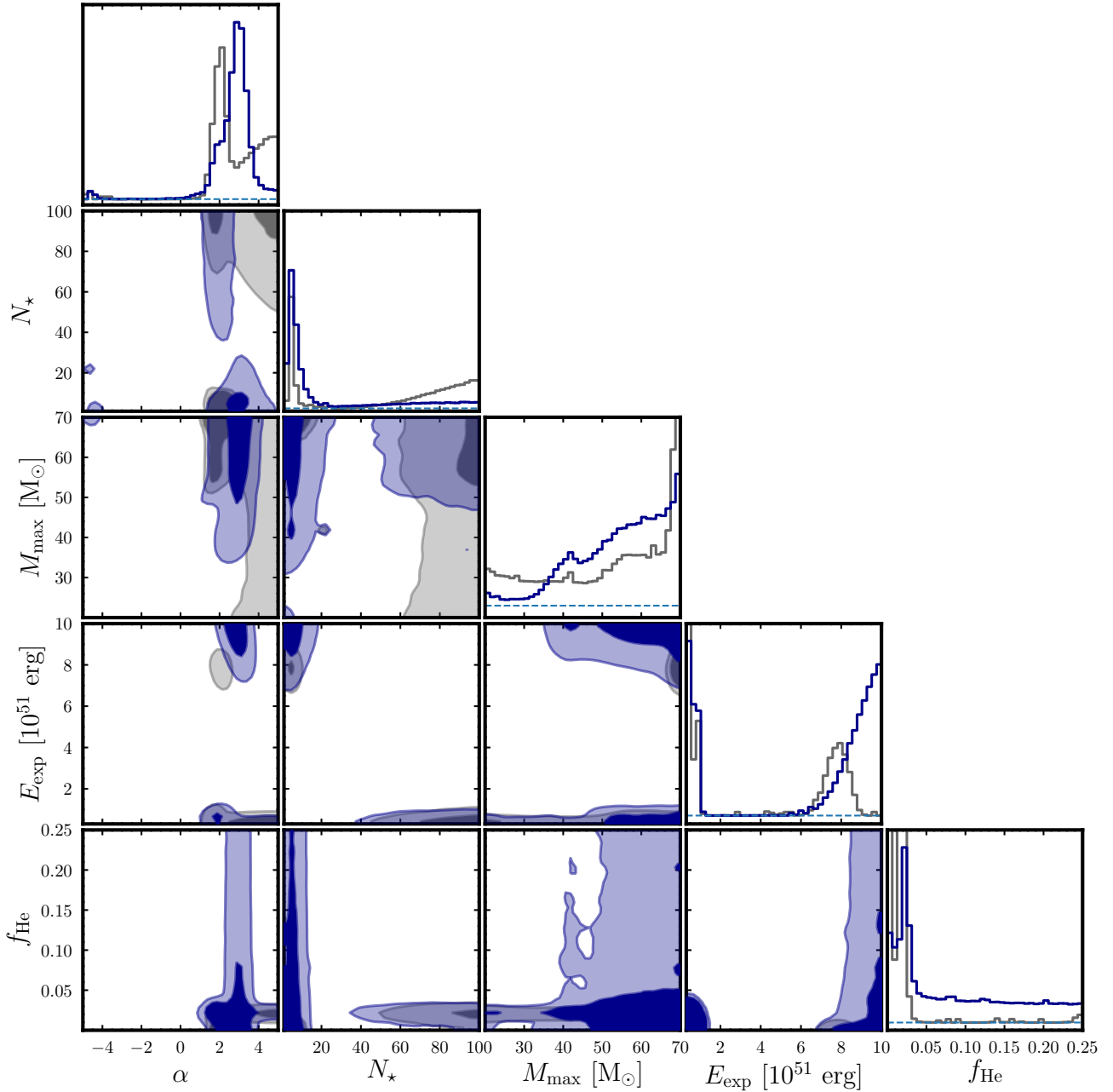
Figure 6. The marginalised maximum likelihood distributions of our stochastic chemical enrichment model parameters (main diagonal), and their associated 2D projections, given the abundances of a sample of metal-poor MW halo stars. The dark and light contours show the 68% and 95% confidence regions of these projections, respectively. The horizontal blue dashed lines in the diagonal panels mark where the individual parameter likelihood distributions fall to zero. The grey distributions correspond to the simultaneous analysis of the stars from C04, B09, Y13, and R14. The blue distributions are the result of removing the R14 data from the sample.

The maximum mass of the enriching stars is unconstrained while the marginalised 1D posterior distribution of $E_{\rm exp}$ tends towards the two extremes; if we consider the scenario with $N_\star < 18$, then we infer $\hat{E}_{\rm exp} > 6$ B (95 per cent confidence). Finally, the preferred mixing prescription is $\hat{f}_{\rm He} = 0.03^{+0.10}_{-0.03}$. Thus, our analysis suggests that the observed abundances of this metal-poor stellar sample are best described by enrichment from a small handful of Pop III hypernovae whose progenitors experienced minimal mixing between the

stellar layers. Additionally, the slope of the underlying IMF (at least for masses that exceed 10 $M_\odot$) is consistent with that of a Salpeter distribution ($\alpha = 2.35$).
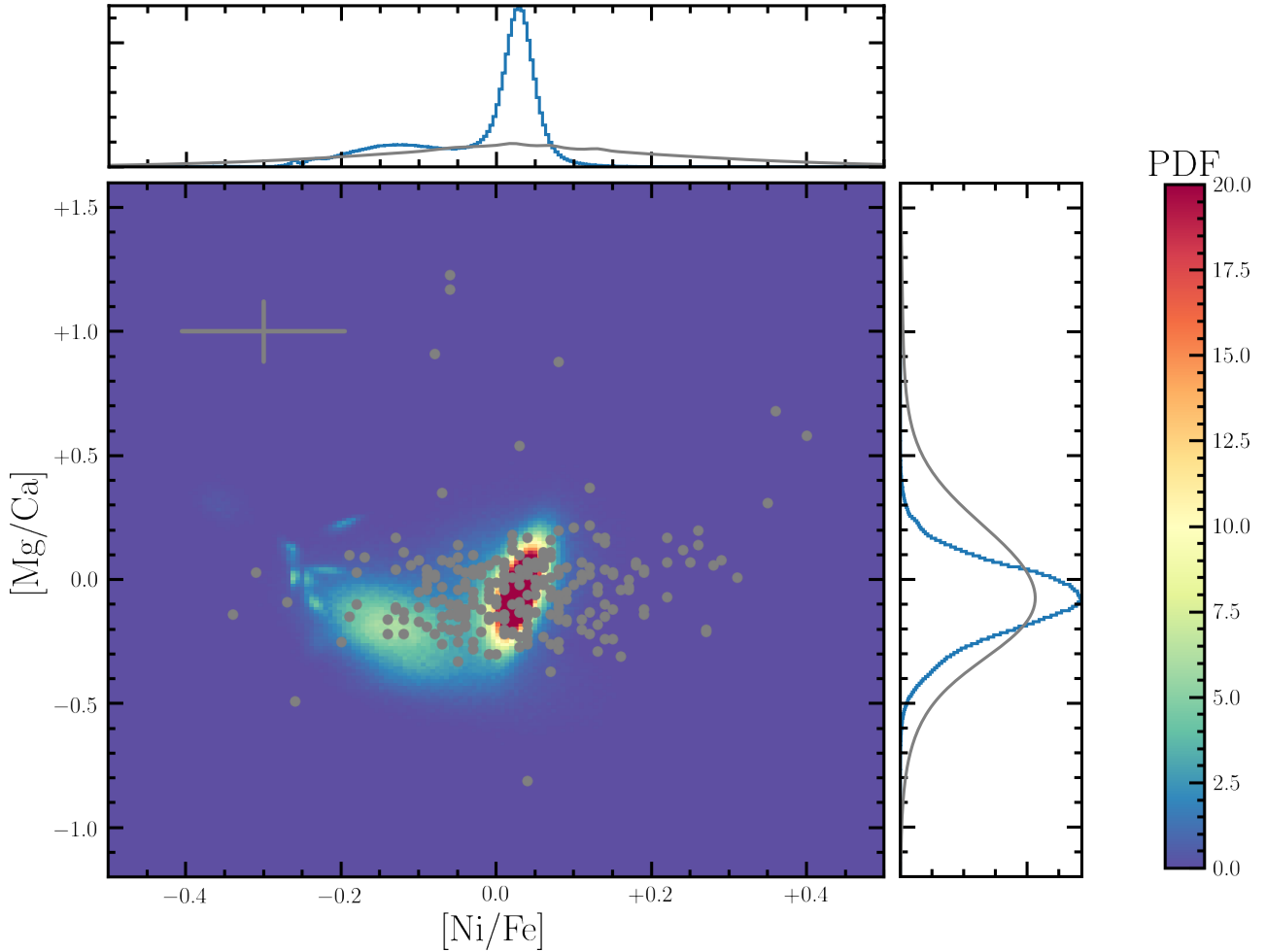
Figure 7. [Mg/Ca] and [Ni/Fe] data of all of the samples with the median error plotted in the top left corner. The background contours highlight the PDF of the expected abundances given our inferred chemical enrichment model. The blue histograms in the top and left panels show the 1D projections of the expected [Ni/Fe] and [Mg/Ca] abundances, respectively, given our inferred enrichment model. The grey curves show the generalised histograms of the data used in our analysis.

5 DISCUSSION

We first investigate the sensitivity of our results to the stellar atmosphere modelling. We then discuss the limitations of our model, and in particular, the chemical yields of massive stars. We close this section by drawing comparisons between the analysis of the most metal-poor stars and DLAs.

5.1 Departures from local thermodynamic equilibrium

One of the assumptions that underpins the observational data is that the absorption lines are all formed in regions of local thermodynamic equilibrium (LTE). Neglecting departures from LTE is common practice when determining the stellar chemical abundances. Including non-LTE processes requires computationally expensive calculations that are generally dependent on the metallicity and surface temperature of the star under consideration, and requires knowledge of the radiative and collisional processes that drive the gas out of LTE. These calculations are unique to the element being considered and, indeed, are also influenced by its initial abundance

(Andrievsky et al. 2010). While difficult to compute, these calculations can improve both the accuracy and the precision of the Mg, Ca, and Ni abundance determinations.

Non-LTE Mg abundances for a subset of our stellar sample have been computed by Andrievsky et al. (2010). The non-LTE corrections to Mg typically increase the Mg abundance by ∼ 0.3 dex. Although non-LTE corrections to Ca are not currently available for the stars considered in this work, we note that the relative correction to the [Mg/Ca] abundances depends on metallicity (Ezzeddine et al. 2018); around [Fe/H] ≃ −3, the [Mg/Ca] abundance should be reduced by ∼ 0.1 dex. Furthermore, this correction becomes more significant at even lower metallicity (Sitnova et al. 2019). Therefore, applying a non-LTE correction to Mg and Ca might bring our model into better agreement with the data. We look forward to a more detailed assessment of the [Mg/Ca] abundances when non-LTE corrections are available for a large fraction of the stellar sample employed in this work.
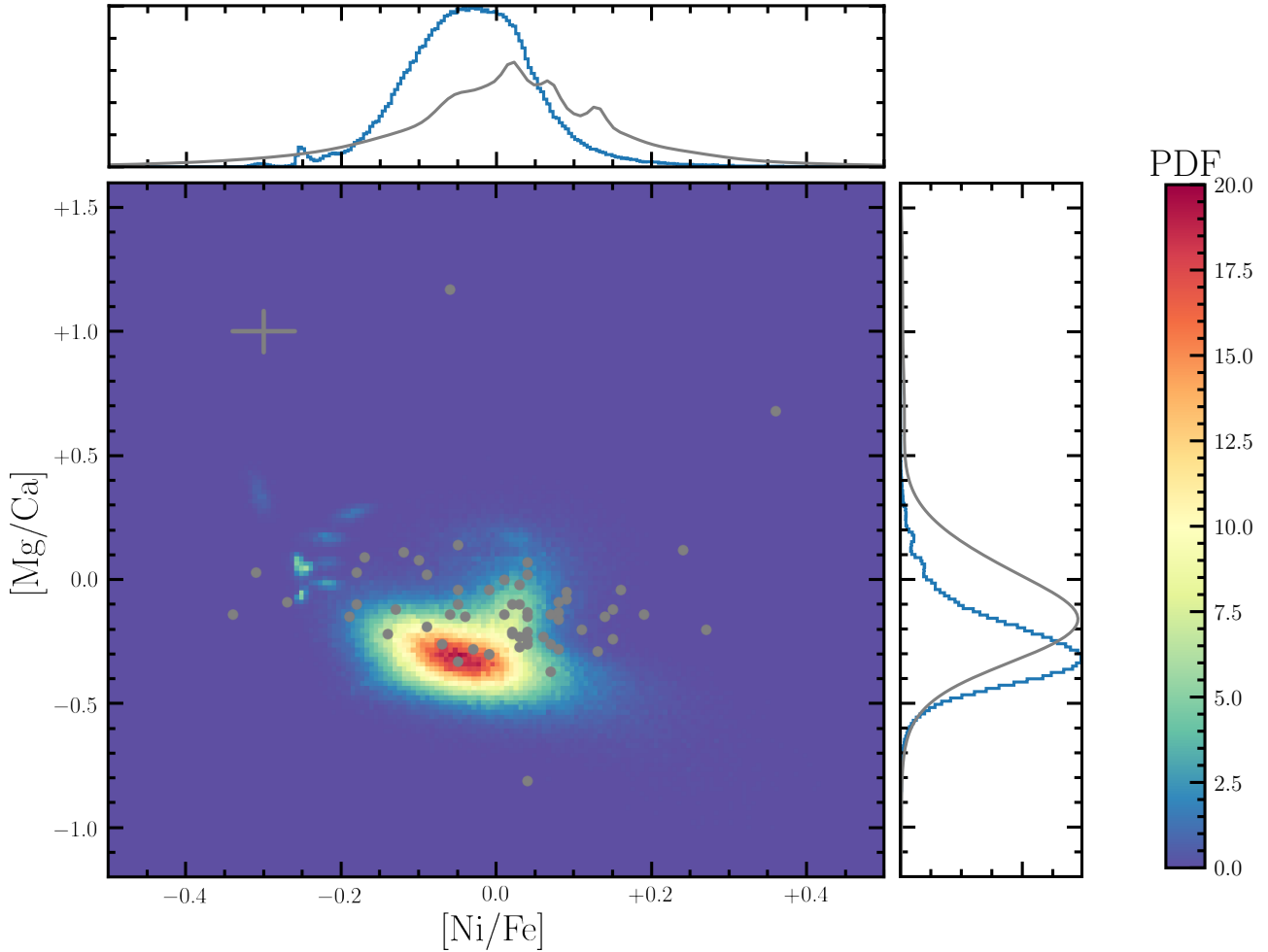
Figure 8. Same as Figure 7 for the case when we exclude the R14 data from our sample.

5.2 Assessment of the yields

We now consider potential improvements that could be made to the nucleosynthetic yields used in our model. As discussed in the previous section, the yields are unable to produce supersolar [Mg/Ca] at the same time as supersolar [Ni/Fe] (see Figures 4 and 7). When removing the R14 data (see Figure 8), the model cannot reproduce the large spread of [Ni/Fe] values; in particular, the highest values of [Ni/Fe] deviate from the best-fit model. Assuming that the observed abundances are reliable, this suggests that either: (1) massive metal-free stars are not the only sources responsible for the chemical enrichment of the most metal-poor stars; or (2) the simulated yields do not fully capture the physics that is necessary to reproduce the observed abundances.

Considering the first possibility, there are a number of alternative sources of enrichment that are not considered in this work. These include low mass metal-free stars (e.g Campbell & Lattanzio 2008), pair instability SNe (PISNe) (e.g. Heger & Woosley 2002), pulsational pair-instability SNe (pPISNe) (e.g. Woosley 2017), and rapidly-rotating near-pristine massive stars (e.g. Meynet et al. 2010). There are reasonable reasons to discount the first three sources, for example: (1) the most metal-poor stars are believed to have formed in the very early universe, when there

would not have been enough time for low and intermediate mass stars to contribute their enrichment. (2) PISNe produce a lot of metals, but their distinct chemical signatures (e.g. a low [α/Fe] ratio, and a strong odd-even effect) are not seen in any of the stars of our sample. Furthermore, the yields of PISNe are expected to be incorporated in stars of metallicity [Fe/H] ~ −2.0 (e.g. Aoki et al. 2014) which is somewhat higher than the stars in our sample. (3) pPISNe also produce a distinct chemical signature (including a very high [α/Fe] ratio). This signature is not observed in any stars of our sample. Finally, although we cannot discount enrichment from the rotating near-pristine stars based on the current data, this may become possible in the future by exploring a larger grid of models or by measuring the helium mass fraction of the stellar sample.

We now consider the possibility that the simulated yields are not yet able to fully capture the physics underpinning the stellar evolution and SN explosions of metal-free stars. In recent years substantial progress has been made in simulating CCSNe in 3D (e.g. Vartanyan et al. 2018). However, the mechanism that drives CCSNe is still unknown. We therefore lack a description of these SNe from first principles, and thus model calculations need to parameterise the explosion model. As discussed in Section 4, the HW10 simulations are performed in 1D using non-rotating

models. Calculations performed in multiple dimensions are better able to capture the impact of both Rayleigh-Taylor instabilities and stellar rotation (Joggerst et al. 2010a,b; Vartanyan et al. 2018). Furthermore, multidimensional models allow for departures from spherical symmetry, providing a more physically motivated scenario. We refer the reader to Müller (2019) for a discussion of potential ways to observationally decipher this explosion mechanism and to Müller (2020) for a review of the state-of-the-art simulations in this field.

Indeed, being able to accurately simulate the complexity of a CCSN is a tall order. Surveys of metal-poor stars (e.g. Starkenburg et al. 2017; Da Costa et al. 2019) are uncovering a slew of chemically peculiar stars whose abundances are challenging to explain through the yields of CCSNe alone. An analysis of the abundances of UMP stars has shown that the HW10 yields are not always sufficient (Placco et al. 2016). Further, the recent detection of elevated Zn in the chemically peculiar star HE 1327-2326 has motivated the consideration of aspherical SNe models (Ezzeddine et al. 2019). We thus conclude that nucleosynthetic yields provide an illustrative model of chemical enrichment, but because of the various simplifications involved, it is not yet clear how accurately the yields will represent the data. Moving forward, we highlight the importance of quantifying the errors of nucleosynthetic yields, and including this uncertainty in the modelling of observational data.

5.3 Comparison with DLAs

A complementary approach to studying the chemistry of stellar relics is the study of minimally processed gas at high redshift (Erni et al. 2006; Pettini et al. 2008; Penprase et al. 2010). There are some gaseous systems at $z \sim 3 - 4$ that appear to show *no* discernible metals (e.g. Fumagalli et al. 2011 and Robert et al. 2019). These systems may have remained *entirely* untouched by the process of star formation. There are other systems, whose metallicities are comparable to that of EMP stars, that may have been solely enriched by the first generation of stars (e.g. Cooke et al. 2017). These systems, defined as DLAs if the column density of neutral hydrogen exceeds $\log_{10} N(\text{H\,{\sc i}})/\text{cm}^{-2} > 20.3$, offer an alternative environment to search for a unique Population III signature.

In contrast to stellar relics, whose abundance determinations require the consideration of complex processes, the physics required to determine the chemical composition of DLAs is rather simple; the column density of neutral hydrogen in these systems is sufficiently high to self-shield the gas, leaving all metals in a single dominant ionisation state. We can therefore determine the elemental abundances of these systems with a high degree of precision (~ 0.01 dex; Wolfe et al. 2005). Additionally, when investigating these systems (as done in Welsh et al. 2019, 2020) we can utilise the abundance ratios of the most abundant chemical elements, including [C/O]. The simulated [C/O] HW10 yields share an almost monotonically decreasing relationship with progenitor star mass. This is invaluable when attempting to estimate the mass distribution of the enriching stars. While the abundances of DLAs are, in principle, more straightforward to determine, these systems do not necessarily probe the multiplicity of the first stars (i.e. the average number of massive Population III stars forming in a given minihalo). Instead, it is possible that the constituent DLA gas has originated from multiple minihaloes. Thus, the combined analysis of both EMP DLAs and EMP stars offers a novel opportunity to investigate the number of minihaloes that have chemically contributed to these high redshift structures (i.e. $N_{\text{halos}} = N_{\star\,\text{DLAs}}/N_{\star\,\text{Pop II}}$).
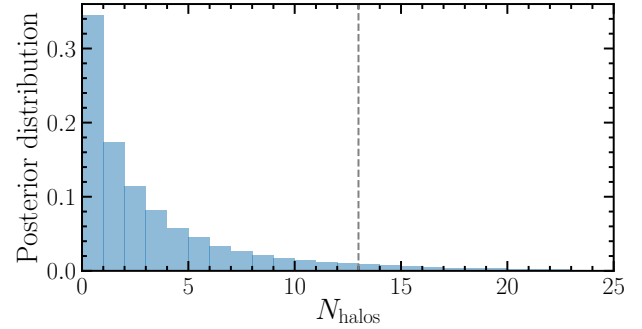
Figure 9. The posterior distribution of the average number of minihaloes that may have chemically contributed to the most metal-poor DLAs given our estimate of $N_{\star\,\text{DLAs}}$ from Welsh et al. 2019 and our estimate of $N_{\star\,\text{Pop II}}$ from this work. The vertical dashed line indicates the 95$^{\text{th}}$ percentile of this distribution and corresponds to our quoted 2σ upper limit.

Given the currently available data and suite of yield calculations, we can estimate the posterior distribution of N_{halos} given the inference on $N_{\star\,\text{DLAs}}$ from Welsh et al. (2019) and $N_{\star\,\text{Pop II}}$ from this work. The results of this comparison are shown in Figure 9 and indicate that the maximum likelihood value of $\hat{N}_{\text{halos}} = 1$. The most metal-poor DLAs may therefore contain the chemical products from just 1 or 2 minihaloes; they could also represent the clouds of gas from which some Population II stars formed. However, the tail of the $N_{\star\,\text{DLAs}}$ distribution is quite broad and we therefore conservatively conclude $N_{\text{halos}} < 13$ (95 per cent confidence). This upper limit is indicated by the vertical dashed line in Figure 9. Given more precise constraints, this tool may provide a test of galaxy formation on the smallest scales. We look forward to comparing the enrichment histories of these systems in detail with future data.

6 CONCLUSIONS

In this paper we have applied a novel stochastic chemical enrichment model to investigate the possible enrichment history of a sample of metal-poor Milky Way halo stars using the [Mg/Ca] and [Ni/Fe] abundances from four historic surveys (C04, B09, Y13, and R14). This is the first analysis to consider the number of massive Population III stars that have chemically enriched these stellar relics. Our main conclusions are as follows:

(i) With the adopted nucleosynthetic yields, our stochastic chemical enrichment model is able to reproduce the observed abundances of a stellar subsample comprising the C04, B09, and Y13 data. In this scenario, our model shows preferential enrichment from a low number of Population III hypernovae.

(ii) Specifically, this model suggests that a typical metal-poor star has been chemically enriched by $\hat{N}_\star = 5^{+13}_{-3}$ Population III hypernovae ($\hat{E}_{\text{exp}} > 6$ B ; 95 per cent confidence) that experienced minimal mixing between the stellar layers ($\hat{f}_{\text{He}} = 0.03^{+0.10}_{-0.03}$). The IMF slope of this enriching population is found to be broadly consistent with that of a Salpeter distribution ($\hat{\alpha} = 2.9^{+0.9}_{-0.6}$). Unless otherwise stated, these errors represent the 68 per cent confidence intervals of our estimates.

(iii) We consider the value of $N_\star$ reported in this paper to be a proxy for the multiplicity of massive Population III stars. By

comparing this result to the $N_\star$ value inferred for the most metal-poor DLAs (see Welsh et al. 2019), we estimate the average number of minihaloes that may have chemically contributed to these low mass structures at $z \sim 2-3$. We find $N_{\text{halos}} < 13$ (95 per cent confidence). The maximum likelihood value of this distribution suggests that the most metal-poor DLAs may contain the chemical products from only a few minihaloes. In future, with more precise constraints, we hope to probe whether these DLAs resemble the gas that some Population II stars formed from.

(iv) In our analysis we utilise the abundance ratios calculated under the assumption of LTE. Recent work considering the non-LTE corrections to the observed [Mg/Ca] abundance ratios of these data may bring our model into better agreement with the data (Ezzeddine et al. 2018; Sitnova et al. 2019). Similarly, the different methods used to infer the effective temperature of the stars in our sample produce a [Mg/Ca] offset of $\sim +0.1$ dex (see the discussion in R14). Although this difference is small, we find that the yields (and our model parameters) are sensitive to these small changes in abundance ratios. Thus, in future analyses, we require abundance measurements reported with an accuracy of ~ 0.05 dex to produce reliable estimates.

(v) We also comment that the various parameterisations involved in nucleosynthetic yield calculations mean that it is not yet clear how accurately the adopted yields capture all of the relevant physics. Going forward, it would be helpful to consider the uncertainties of the simulated yields in future analyses.

Finally, we emphasis that utilising this model to investigate the enrichment of both Population II stars and the *most* metal-poor DLAs may reveal, not only the multiplicity of the first stars, but the chemical enrichment of some of the lowest mass structures at $z \sim 3$. It is therefore a promising tool for investigating early structure formation. Future modifications to this model may offer an alternative way to study inhomogeneous metal-mixing and the possibility of externally enriched minihaloes.

DATA AVAILABILITY

No new data were generated or analysed in support of this research.

REFERENCES

Abel T., Bryan G. L., Norman M. L., 2002, Science, 295, 93

Aguado D. S., Allende Prieto C., González Hernández J. I., Carrera R., Rebolo R., Shetrone M., Lambert D. L., Fernández-Alvar E., 2016, A&A, 593, A10

Andrievsky S. M., Spite M., Korotin S. A., Spite F., Bonifacio P., Cayrel R., François P., Hill V., 2010, A&A, 509, A88

Aoki W., et al., 2013, AJ, 145, 13

Aoki W., Tominaga N., Beers T. C., Honda S., Lee Y. S., 2014, Science, 345, 912

Asplund M., 2005, ARA&A, 43, 481

Asplund M., Grevesse N., Sauval A. J., Scott P., 2009, ARA&A, 47, 481

Barkana R., Loeb A., 2001, Phys. Rep., 349, 125

Bastian N., Covey K. R., Meyer M. R., 2010, ARA&A, 48, 339

Beers T. C., Christlieb N., 2005, ARA&A, 43, 531

Beers T. C., Preston G. W., Shectman S. A., 1985, AJ, 90, 2089

Beers T. C., Preston G. W., Shectman S. A., 1992, AJ, 103, 1987

Bond H. E., 1980, The Astrophysical Journal Supplement Series, 44, 517

Bonifacio P., et al., 2009, A&A, 501, 519

Bromm V., Yoshida N., 2011, ARA&A, 49, 373

Bromm V., Coppi P. S., Larson R. B., 2002, ApJ, 564, 23

Bromm V., Yoshida N., Hernquist L., 2003, ApJ, 596, L135

Caffau E., et al., 2013, A&A, 560, A71

Campbell S. W., Lattanzio J. C., 2008, A&A, 490, 769

Cayrel R., et al., 2004, A&A, 416, 1117

Chieffi A., Limongi M., 2004, ApJ, 608, 405

Christlieb N., Schörck T., Frebel A., Beers T. C., Wisotzki L., Reimers D., 2008, A&A, 484, 721

Clark P. C., Glover S. C. O., Klessen R. S., 2008, ApJ, 672, 757

Clark P. C., Glover S. C. O., Klessen R. S., Bromm V., 2011, ApJ, 727, 110

Cooke R. J., Pettini M., Steidel C. C., 2017, MNRAS, 467, 802

Da Costa G. S., et al., 2019, MNRAS, 489, 5900

Erni P., Richter P., Ledoux C., Petitjean P., 2006, A&A, 451, 19

Ezzeddine R., Sitnova T., Frebel A., Mashonkina L., Plez B., 2018, in Chiappini C., Minchev I., Starkenburg E., Valentini M., eds, IAU Symposium Vol. 334, Rediscovering Our Galaxy. pp 259–262, doi:10.1017/S1743921317007177

Ezzeddine R., et al., 2019, ApJ, 876, 97

Foreman-Mackey D., Hogg D. W., Lang D., Goodman J., 2013, PASP, 125, 306

Frebel A., 2010, Astronomische Nachrichten, 331, 474

Frebel A., Norris J. E., 2015, ARA&A, 53, 631

Frebel A., Chiti A., Ji A. P., Jacobson H. R., Placco V. M., 2015, ApJ, 810, L27

Fumagalli M., O'Meara J. M., Prochaska J. X., 2011, Science, 334, 1245

Greif T. H., Glover S. C. O., Bromm V., Klessen R. S., 2010, ApJ, 716, 510

Greif T. H., White S. D. M., Klessen R. S., Springel V., 2011, ApJ, 736, 147

Greif T. H., Bromm V., Clark P. C., Glover S. C. O., Smith R. J., Klessen R. S., Yoshida N., Springel V., 2012, MNRAS, 424, 399

Hartwig T., Yoshida N., 2019, ApJ, 870, L3

Hartwig T., Ishigaki M. N., Klessen R. S., Yoshida N., 2018a, MNRAS,

Hartwig T., et al., 2018b, MNRAS, 478, 1795

Heger A., Woosley S. E., 2002, ApJ, 567, 532

Heger A., Woosley S. E., 2010, ApJ, 724, 341

Howes L. M., et al., 2016, MNRAS, 460, 884

Ishigaki M. N., Tominaga N., Kobayashi C., Nomoto K., 2018, ApJ, 857, 46

Ji A. P., Frebel A., Bromm V., 2015, MNRAS, 454, 659

Joggerst C. C., Almgren A., Bell J., Heger A., Whalen D., Woosley S. E., 2010a, ApJ, 709, 11

Joggerst C. C., Almgren A., Woosley S. E., 2010b, ApJ, 723, 353

Karlsson T., 2005, A&A, 439, 93

Karlsson T., Gustafsson B., 2005, A&A, 436, 879

Keller S. C., et al., 2007, Publ. Astron. Soc. Australia, 24, 1

Li H.-N., Zhao G., Christlieb N., Wang L., Wang W., Zhang Y., Hou Y., Yuan H., 2015, ApJ, 798, 110

Limongi M., Chieffi A., 2012, The Astrophysical Journal Supplement Series, 199, 38

Meynet G., Hirschi R., Ekstrom S., Maeder A., Georgy C., Eggenberger P., Chiappini C., 2010, A&A, 521, A30

Müller B., 2019, Annual Review of Nuclear and Particle Science, 69, annurev

Müller B., 2020, Living Reviews in Computational Astrophysics, 6, 3

Naoz S., Yoshida N., Gnedin N. Y., 2012, ApJ, 747, 128

Nordlander T., et al., 2019, MNRAS, 488, L109

Penprase B. E., Prochaska J. X., Sargent W. L. W., Toro-Martinez I., Beeler D. J., 2010, ApJ, 721, 1

Pettini M., Zych B. J., Steidel C. C., Chaffee F. H., 2008, MNRAS, 385, 2011

Placco V. M., et al., 2016, ApJ, 833, 21

Robert P. F., Murphy M. T., O'Meara J. M., Crighton N. H. M., Fumagalli M., 2019, MNRAS, 483, 2736

Roederer I. U., Preston G. W., Thompson I. B., Shectman S. A., Sneden C., Burley G. S., Kelson D. D., 2014, AJ, 147, 136

Salpeter E. E., 1955, ApJ, 121, 161

Salvadori S., Ferrara A., Schneider R., Scannapieco E., Kawata D., 2010, MNRAS, 401, L5

Sarmento R., Scannapieco E., Pan L., 2017, ApJ, 834, 23

Sitnova T. M., Mashonkina L. I., Ezzeddine R., Frebel A., 2019, MNRAS, 485, 3527

Stacy A., Greif T. H., Bromm V., 2010, MNRAS, 403, 45

Stacy A., Bromm V., Lee A. T., 2016, MNRAS, 462, 1307

Starkenburg E., et al., 2017, MNRAS, 471, 2587

Suda T., et al., 2008, PASJ, 60, 1159

Suda T., Yamada S., Katsuta Y., Komiya Y., Ishizuka C., Aoki W., Fujimoto M. Y., 2011, MNRAS, 412, 843

Suda T., et al., 2017, PASJ, 69, 76

Susa H., Hasegawa K., Tominaga N., 2014, ApJ, 792, 32

Tarumi Y., Hartwig T., Magg M., 2020, arXiv e-prints, p. arXiv:2005.10401

Thévenin F., Idiart T. P., 1999, ApJ, 521, 753

Tominaga N., Umeda H., Nomoto K., 2007, ApJ, 660, 516

Umeda H., Nomoto K., 2002, ApJ, 565, 385

Umeda H., Nomoto K., 2003, Nature, 422, 871

Umeda H., Nomoto K., 2005, ApJ, 619, 427

Vartanyan D., Burrows A., Radice D., Skinner M. A., Dolence J., 2018, MNRAS, p. 2479

Welsh L., Cooke R., Fumagalli M., 2019, MNRAS, 487, 3363

Welsh L., Cooke R., Fumagalli M., Pettini M., 2020, MNRAS, 494, 1411

Wolfe A. M., Gawiser E., Prochaska J. X., 2005, ARA&A, 43, 861

Woosley S. E., 2017, ApJ, 836, 244

Woosley S. E., Weaver T. A., 1995, ApJS, 101, 181

Yamada S., Suda T., Komiya Y., Aoki W., Fujimoto M. Y., 2013, MNRAS, 436, 1362

Yong D., et al., 2013, ApJ, 762, 26

This paper has been typeset from a TeX/LaTeX file prepared by the author.

APPENDIX A: INTRINSIC SCATTER CALCULATION

In this appendix, we describe our approach to estimate the intrinsic scatter of the stellar samples. This scatter is defined by Eq. 1. As described in Section 3, we consider two model parameters ([X/Fe]$_{cent}$ and σ_{int}) that we determine independently for each abundance ratio and each sample. We use an MCMC procedure to simultaneously estimate the central values [Mg/Fe]$_{cent}$, [Ca/Fe]$_{cent}$, and [Ni/Fe]$_{cent}$ of a sample, alongside their associated additional error components $\sigma_{int,Mg}$, $\sigma_{int,Ca}$, and $\sigma_{int,Ni}$. We adopt uniform priors for these parameters; the central values are bounded by $-5 \leq [X/Fe]_{cent} \leq 5$ and the intrinsic errors are bounded by $0 \leq \sigma_{int,X} \leq 5$. We utilised the EMCEE software package (Foreman-Mackey et al. 2013) to randomly initialise 400 walkers and explore this parameter space. The results of this analysis for the C04 data are presented in Figure A1 which shows the converged posterior distributions of these model parameters. The confidence interval for [Mg/Fe] demonstrates there is a statistically significant deviation from 0; this result is replicated across all of the stellar samples. We consider the possibility that this intrinsic dispersion is the result of stochastic sampling of the IMF.
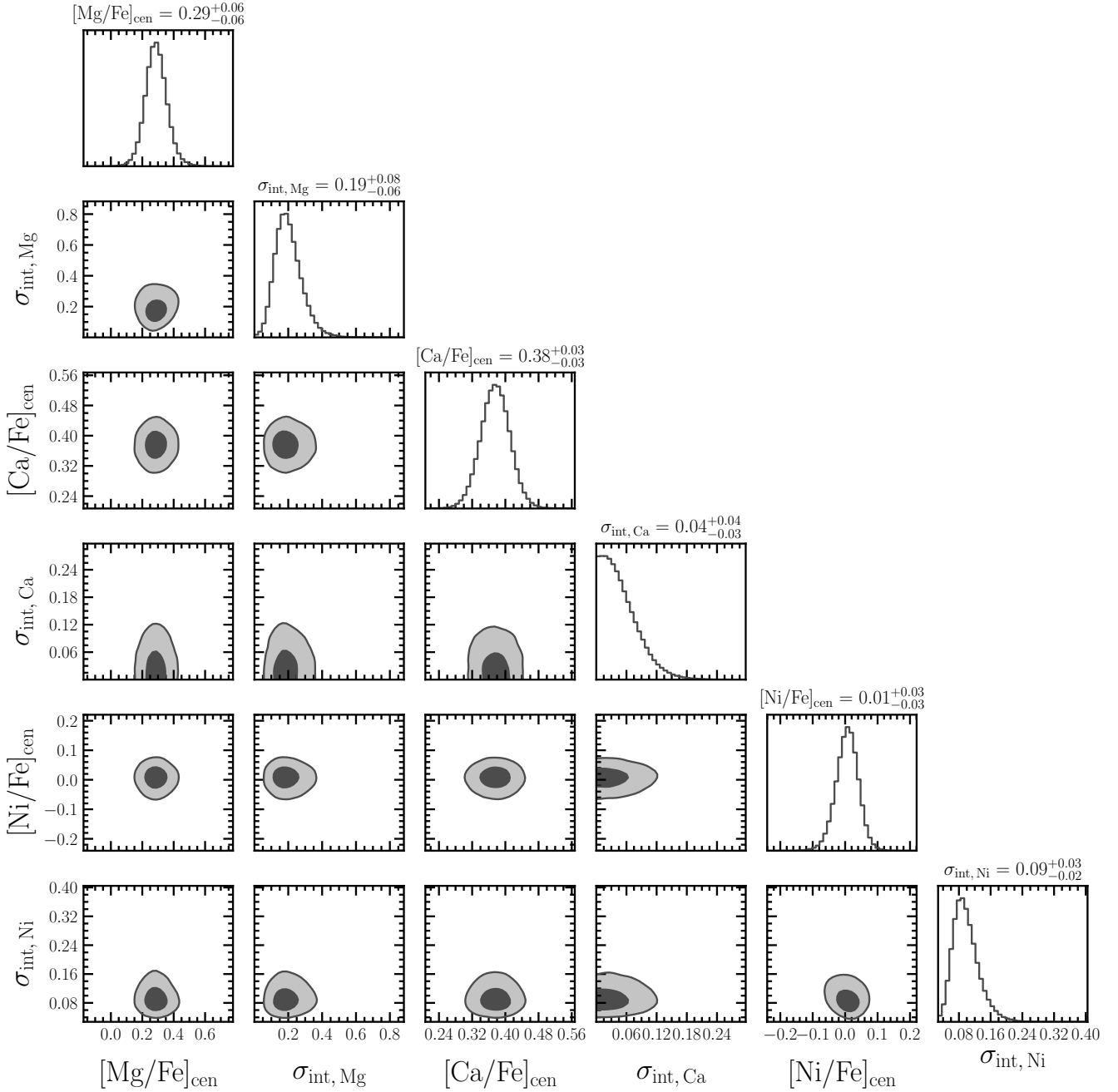
Figure A1. Converged MCMC analysis of the intrinsic scatter of the C04 data. The main diagonal panels show the marginalised maximum likelihood distributions of the parameters describing the central values and intrinsic dispersions of the C04 data (refer to Section 3). The associated contours highlight their associated 2D projections. The dark and light contours show the 68% and 95% confidence regions of these projections, respectively.